The "Slugs-test" for extrusion-based additive manufacturing: Protocol, analysis and practical limits

Nicolas Ducoulombier, Romain Mesnil, Paul Carneau, Léo Demont, Hela Bessaies-Bey, Jean-François Caron, Nicolas Roussel

The "Slugs-Test" for extrusion-based additive manufacturing : Protocol, analysis and practical limits

Nicolas Ducoulombier[b,*], Romain Mesnil[c], Paul Carneau[b], Léo Demont[b], Hela Bessaies-Bey[a], Jean-François Caron[b], Nicolas Roussel[b]

[a] *Université Gustave Eiffel, Marne-la-Vallée F-77455, France*
[b] *Navier Laboratory, École des Ponts ParisTech, Univ. Gustave Eiffel, CNRS, Marne-La-Vallée, France*
[c] *École des Ponts ParisTech, Marne-La-Vallée, France*

Abstract

This paper introduces a novel rheological technique allowing for the assessment of printable materials yield stress at nozzle exit in the case of extrusion-based 3D printing. This technique is derived from the analysis of the specific gravity-induced non-Newtonian flow that takes place at nozzle exit, which is at the origin of the formation of material drops or so-called slugs. A simple connected balance located below the nozzle gives access to the slugs mass distribution, the average value and the variability of which allow for the computation of the yield stress and, in parallel, for the assessment of the material homogeneity. In this paper, this method is first experimentally validated on simple materials in simple extruders before it is applied to a real printing system. The equations allowing for the yield stress computation are derived. The accuracy of the technique and its range of applicability are discussed.

Keywords: Extrusion-based additive manufacturing, rheological apparatus, concrete 3D-printing, yield stress assessment

1. Introduction

Concrete 3D-printing or more specifically extrusion-based additive manufacturing of cement-based materials is a very promising way to manufacture construction elements. In reality, this processing technology gathers various

*Corresponding author
E-mail: nicolas .ducoulombier@enpc.fr

kinds of processes, differing essentially on various deposition strategies that have recently been classified in literature [1, 2, 3, 4] and are shown in figure 1.

On one hand, slip forming refers to a family of extrusion processes, belonging to a formative manufacturing technique, where the extrusion length scale is similar to the object length scale, which is not necessarily an additive processes by nature. We specifically refer here to the digital variation around traditional concrete slip forming which can then be seen as an additive manufacturing technique. The present paper however focuses on processes where the extrusion length scale is much smaller than the object length scale. Printed objects result therefore from a progressive layering process. The first of these printing strategies is called "infinite brick extrusion". The cross section of the layer or filament directly relates to the nozzle geometry, the material yield stress at the nozzle being high enough for the filament to remain undeformed after deposition [3]. The second strategy is called free-flow deposition. The filament shape is, in this case, independent of the nozzle shape and results from a competition between gravitational forces and yield stress [3]. Finally, in the third strategy, called Oriented Pressing, the filament shape at the nozzle exit is imposed by the distance between the nozzle and the support (or the previous layer) as the extrusion velocity is slightly higher than the nozzle velocity. This last strategy often allows for a better geometrical control on the final printed object, but induces an additional stress acting on the previous layers that is roughly proportional to the yield stress of the printed material [5]. As a consequence, the value of the yield stress at the nozzle should be sufficiently low. Moreover, in oriented pressing, the yield stress requirement at the nozzle exit highly depends on the support or nozzle orientation [6].

From the above, it can be concluded that, depending on the deposition method, requirements on the yield stress value at the nozzle can significantly vary. It is therefore obviously needed for the sake of process quality control to have a kind of yield stress assessment at the nozzle level. Furthermore, note that for certain reinforcement application [7], the yield stress has a great impact on the impregnation of the reinforcement, thus, on the final interface properties

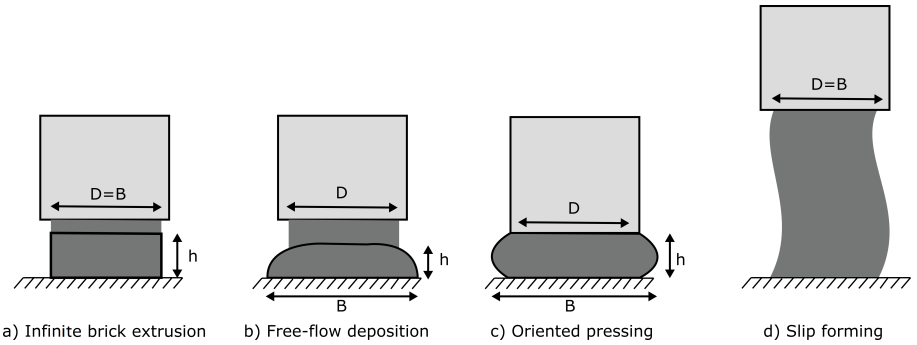

Figure 1: Different deposition strategies for Extrusion-based additive manufacturing, D is the nozzle diameter and B the filament width after deposition.

between fibers and concrete.

Such a measurement is however difficult to achieve, especially for the high structuration rate materials needed for a fast fabrication of slender post-like structure, such as the one presented in [8]. The high structuration rate was, in this case as in many other cases, provided by the addition and dispersion of a chemical accelerator in the printing head [9]. This high structuration rate prevents from sampling the material directly from the nozzle and assess it using standard rheological tests such as slump as the time needed to prepare the sample induces a drastic change in the material yield stress. Another possibility would be to assess yield stress from pressure measurements and pressure sensors located in the nozzle but such a measurement would give information on tribological properties (i.e. the behavior of the layer of material in contact with the nozzle inner wall) rather than information on the material bulk yield stress. Alternatively, some authors [10] suggested to perform ultrasonic pulse velocity test to evaluate the elastic properties at the nozzle level. This however only provides qualitative information, unless proper calibration procedures are carried out for each single printable mixture.

The present paper focuses on another method called "the Slugs-test" allowing for an inline yield stress assessment at the nozzle exit. Its founding principles were introduced in [8]. The present paper aims at generalizing the

analysis, strengthening the validation and providing a specific protocol along with the practical limits of such a rheological tool. The first section introduces the main concept and the theoretical analysis. The second section presents the experimental devices and a preliminary protocol. The third section discusses the ability of the proposed methodology to assess yield stress through a comparison between theory and experiments. The resulting discussion finally leads to the proposal of a generic protocol allowing for yield stress assessment at the nozzle level.

2. Original concept and notations

The original idea comes from the observation of the specific gravity-induced non-Newtonian flow that takes place at the nozzle exit of our printing head, which may result in the formation of material drops or so-called "slugs" [8]. This phenomenon typically takes place at the nozzle exit when the nozzle is still far above the ground and the yield stress is sufficiently high. The exact conditions required for the occurrence of this phenomenon at the nozzle exit are studied further in this paper. The notations used in this paper are given in figure 2-a. Moreover, as shown in figure 2-b,c,d, first observations showed that higher accelerator content, which is expected to lead to higher yield stress, goes with longer (or heavier) slugs.

2.1. General Analysis of the Slugs-test

Similar discontinuous flow during vertical extrusion of food-industry yield stress fluids such as ketchup or mayonnaise were already observed and analysed in literature [11]. These authors demonstrated that the slug mass is mainly controlled by yield stress and eventually by viscosity, while surface tension can often be neglected in front of yield stress. They moreover provided a theoretical framework for Herschel-Bulkley visco-plastic fluids. If τ_c, K and n, are the yield stress, the consistency and the flow index of the Herschel-Bulkley fluid respectively, the formation of drops is driven by the following dimensionless

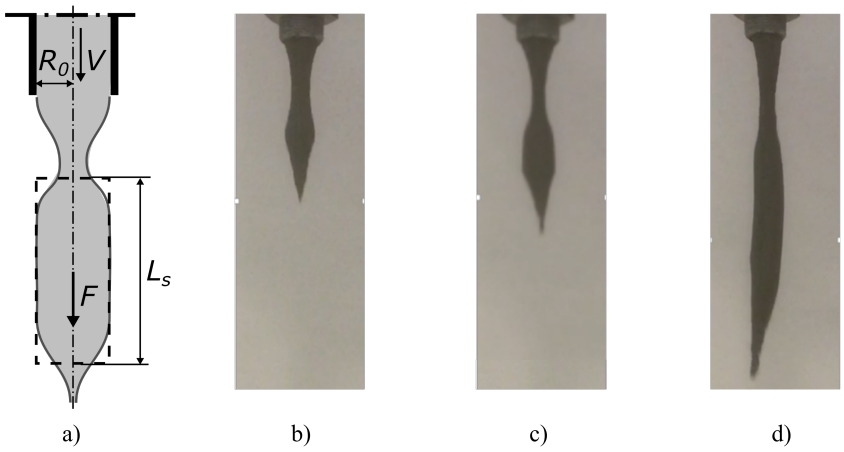

Figure 2: Formation of slugs through necking processes: a) Geometry and notations of the problem, b) experiments at low accelerator contents, b) at median accelerator contents, d) at high accelerator contents

relation :

$$\lambda\left(\lambda-1\right)^{1/n}=\nu \tag{1}$$

where $\lambda=\rho g L_s/(\sqrt{3}\tau_c)$ is the dimensionless length of the slugs,

and $\nu=(K/\tau_c)^{1/n}\rho g V/\tau_c$ is the dimensionless extrusion speed. Note also that L_s, g , ρ and V are respectively the dimensional slug length, the gravitational constant on earth, the volume mass of the material and the material speed at the nozzle exit.

We first consider here the case where the extruded material is a pure plastic yield stress fluid (i.e. no viscous contribution). In this simplified case, the viscosity part of the equation vanishes and the slug length L_s only depends on the yield stress. Using the international system of units, reorganising the term and expressing the slug length from the slug mass m_s, the yield stress can then be expressed as:

$$\tau_c=\frac{g}{\sqrt{3}S}m_s \tag{2}$$

where S is the nozzle section ($=\pi {R_0}^2$ in our case), g the earth gravitational constant, $m_s=\rho S L_s$ the slug mass where L_s is the slug length.

Please note that Equation (2) applies when the elastic domain is bounded by a von Mises plasticity criterion for any nozzle shape. The right-hand term is indeed simply the expression of the von Mises stress when the flow is purely extensional (i.e. no shear stresses) at nozzle exit under self-weight ($F = m_s g$).

Despite the wide use of von Mises criterion for printable mixtures at fresh state, it has to be noted that some stiff printable materials were shown to be better described using a Mohr-Coulomb yield function [12].

3. Materials, Experimental devices and protocol

The protocol requires an extrusion device, a scale and a container. In this paper, the experimental validation is made using printable mortar. In a first part, the material was processed manually using a simple extrusion device and a traditional scale while, in a second part, the material is tested using an automated protocol, which was developed, integrated and used in our 3D-printing facility.

3.1. Manual Slugs test

For the first part of the experimental validation, a specific extrusion device shown on figure 3 was equipped with a 10 mm-diameter nozzle. Using the relation 2, yield stress assessment is performed by collecting around 30 slugs and measuring the total mass of extruded material. Introducing m_t the total collected mass and n the number of slugs, the slug mass is estimated by the empirical mean $m_s = m_t/n$. Note that uncertainties can be estimated in this case using k successive experiments. Here, four successive experiments collecting seven slugs.

3.2. Automated Slugs test

In the context of a real application in our 3D-printing facilities, a specific device was developed by connecting the load sensor of a scale to a computer via a standard acquisition card as shown in figure 4. This automated slugs-test was

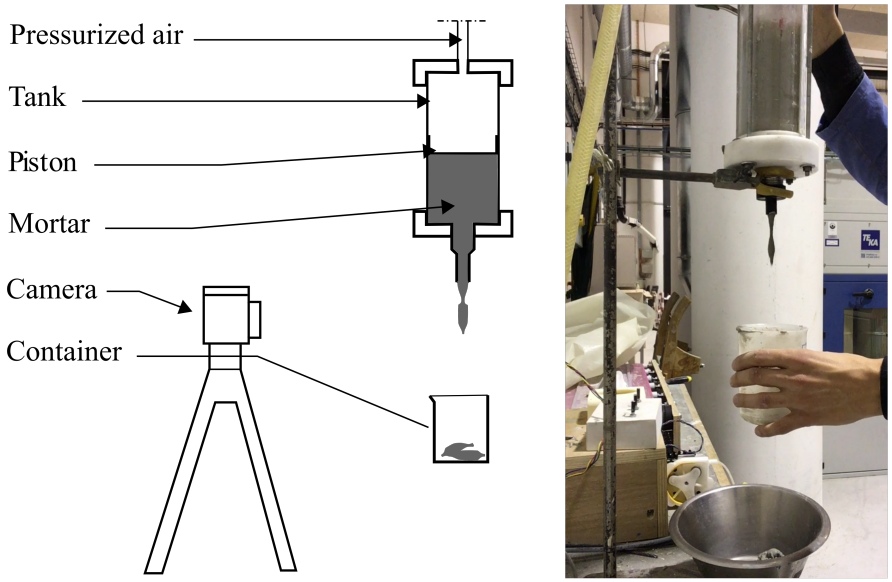

Figure 3: Simple extruder developed for the first part of the experimental validation

positioned below our printing head equipped with a 20-mm diameter nozzle and is used here for the second part of the experimental validation.

A typical acquisition is illustrated in figure 5. The observed discontinuous flow results in a step-wise measured mass evolution with time as shown by the orange curve in the top graph, where each step corresponds to a new slug. An appropriate discrete derivation of the signal yields to the green signal where a threshold filter shown in the yellow curve allows for the slug impacts detection. Finally, the mass of each individual slugs is computed from the differences between each consecutive step. Consequently, both yield stress mean value can be automatically computed using equation (2), while the n slugs correspond to n successive measurements and allow for the estimation of the test uncertainties. In this paper, a 95% confidence interval is considered, postulating normally distributed slugs masses. The details of the assessment of the confidence interval are given in section 4.5.

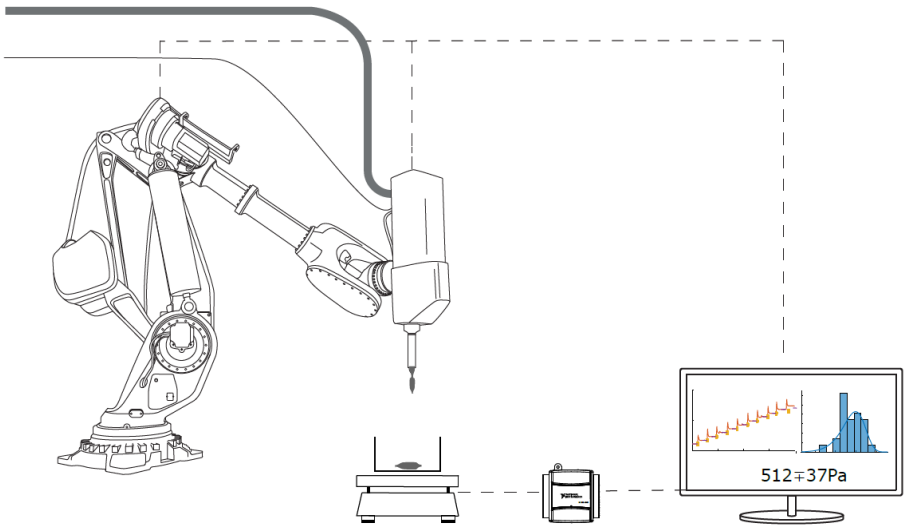

Figure 4: Automated devices integrated in the Build'in facilities of Ecole des Ponts Paristech

3.3. Materials

The mortar used in this work is formulated using the 3D-CP 90 MPa premix provided by LafargeHolcim. The different yield stress values are obtained by modifying water and superplasticizer contents for the manual slugs test or by replacing the accelerator traditionally dispersed in our printing head as described in [9] by a flocculent additive, a 6-gram-per-liter aqueous solution of polyacrylamide (PAM) (see table 1 for more precision). Its effect on the rheology was already well-described in [13]. Note that 6-mm long glass fibres are added in the formulation of the automated slug test in proportion similar to the usual formulation used for 3D printing in the *Build'in* platform of Ecole des Ponts ParisTech. The mixing procedure is made by a 5-liter mixing unit for the manual slug test and a 100-liter mixer for the automated slug test. First, the premix is added in the mixer. Then, the water and superplasticizer are added at small rotation speed during 30 seconds, followed by the insertion of the glass fibres (when needed) after obtaining an homogeneous paste. Finally, the mixing is made at the maximum rotation speed during five minutes.

For the sake of comparison, the yield stress of each mix is also measured

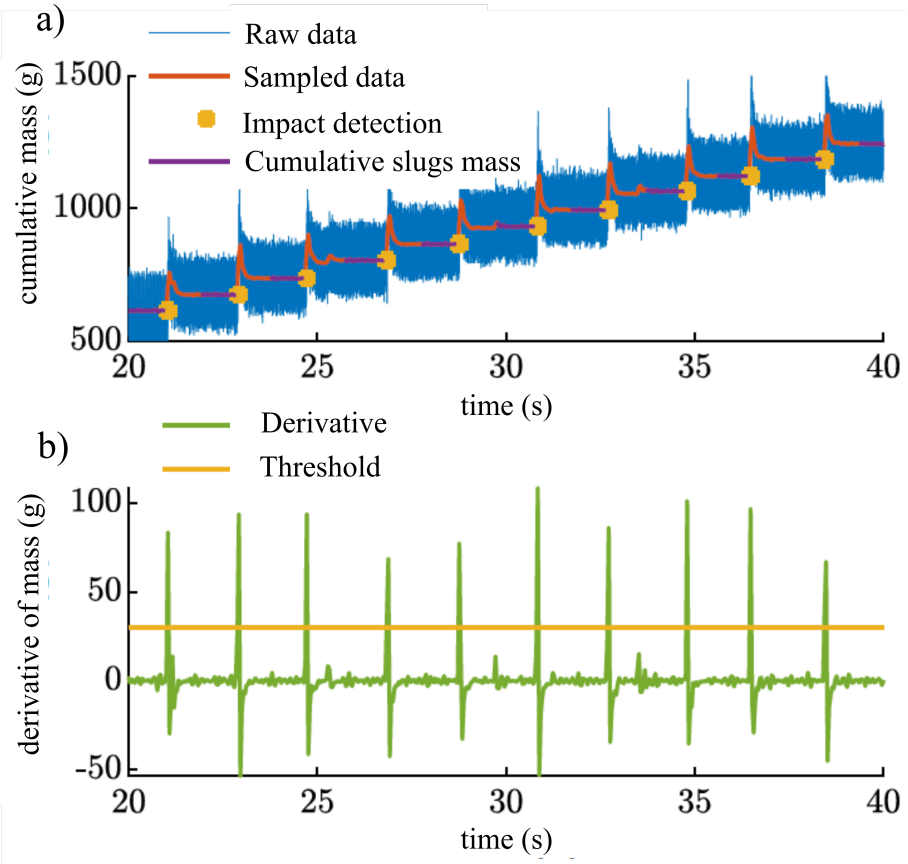

Figure 5: Example of an automated acquisition: a) Cumulative mass obtained by the automatized system b) Derivative of the mass and threshold for impacts detection

Device	Manual Slugs test			Automated Slugs test			
mix number	1	2	3	4	5	6	7
Premix (kg)	1	1	1	1	1	1	1
Glass fibre (g)	-	-	-	-	-	4	4
Water (g)	105	105	105	96	96	96	96
Fluid Optima 100 (g)	3.7	3	3	4.3	4.6	4.3	4.3
Polyacrylamide (PAM) (g)	-	-	-	-	-	6	7.5
Mass flow rate (g/s)	3.5	3.9	3.3	7	15	12	22
Slump τ_c (Pa)	170	260	500	300	190	410	1380
Uncertainties (Pa)	40	50	100	60	50	80	70
Number of experiments / Slugs	4	4	4	24	30	22	39
Slug τ_c (Pa)	210	290	530	350	270	400	1353
Standard deviation (Pa)	9.4	11.1	34.7	50	44	120	190
Variation coefficient (%)	4.5	4	6.5	11.5	16.2	30	14
Uncertainties (Pa)	10	11	34	20	20	50	60

Table 1: Material formulations and experimental results

using a slump test. In the case of the manual slugs-test defined above, the slump test is performed using a 0.28-Liter cone before filling the tank (with a bottom diameter of 90 millimeters, upper diameter of 40 millimeters and a height of 80 millimeters). The yield stresses were then calculated using the asymptotic solution provided in [14]. On the other hand, when the slugs-test are performed using the automated device of our 3D printing facilities, the standard Abrams cone is filled with the extruded material directly from the nozzle. The yield stress is then estimated using the numerical solution provided by [14]. Note moreover that the comparison with slump test is valid here because no accelerator is added to the material. We can therefore expect that the sampled material does not change much between its nozzle outflow and the test. This however reaches a limit as the filling of the 6-liter Abrams cone took from six to twenty minutes depending on flow rate. A slight increase in consistency was therefore visually noticeable between the beginning and the end of the filling process.

4. Results and discussions

4.1. Comparison between theory and experiments

In figure 6, the yield stresses computed from the slugs mass are plotted against the yield stresses computed from the slump measurements. Both yield stresses are also provided in table 1. One can notice the good correlation between yield stresses assessed using slump test and values obtained from both automatic and manual slugs tests, showing that the slugs-test gives a good estimation of the yield stress at the nozzle level.

An interesting discussion concerns the validity of the assumption that the mortar at the nozzle is a pure plastic material. In reality, the analysis for Herschel-Buckley fluid [11] suggests that this simplifying assumption should lead to an overestimation of the yield stress when the viscosity effects cannot be neglected. This is in qualitative agreement with the present graph, where the yield stress computed from the slugs at low yield stresses is systematically

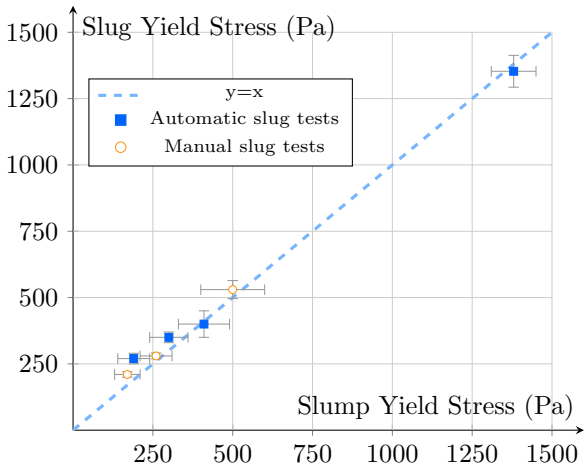

Figure 6: Comparison of yield stresses obtained from Slugs tests versus slump test. The dashed line is the line $y = x$, closeness of experimental points to the line indicate good correlation between the proposed slug test and the classical slump test.

higher than the yield stress computed from the slump. Indeed, it is at low yield stress that the viscous contribution is expected to play a role. A more quantitative estimation of the validity of the above assumption can be obtained by considering the printed mortar as a Bingham model introducing the plastic viscosity μ_p. In this case, equation (1) has one positive analytical solution, which writes:

$$\lambda_b = \frac{1 + \sqrt{1 + 4\nu}}{2} \tag{3}$$

with $\nu = \rho g \mu_p V / \tau_c^2$.

The overestimation can be computed, noting that $\lambda_p = 1$ corresponds to the case of a perfectly plastic material. It yields :

$$\delta = \frac{\lambda_b - \lambda_p}{\lambda_b} = \frac{\sqrt{1 + 4\nu} - 1}{\sqrt{1 + 4\nu} + 1} \tag{4}$$

The figure 7 gives the error made when neglecting viscosity. In most 3d printing process, the extrusion velocity is often of the same order as the nozzle velocity (nominal extrusion or quasi-nominal extrusion), the value of the latter being around 100 mm/s. Note that, due to the volume conservation, the corresponding flow rate Q then only depends on the size of the nozzle: $Q = V * S$. Furthermore,

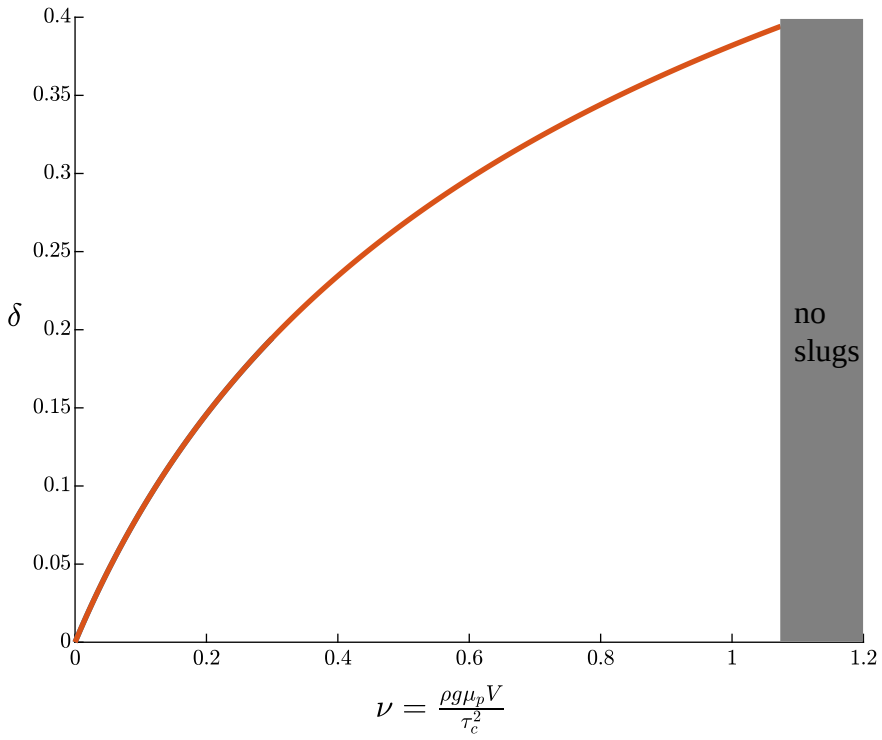

Figure 7: Error, noted δ, made on the yield stress value when neglecting viscosity

the filament thickness is usually higher than 5 millimeters and density of the mixture is around 2200 kg/m^3. The yield stress of any printable mortar is then expected to be superior to 300 Pa ($\tau_c > \rho g h$ [3]). Using those values, ν should remain inferior to 0.2 if the viscosity is taken to be inferior to 10 Pa.s. Then, the figure 7 indicates that neglecting viscous effects shall never induce an error higher than 15%. Please note that, in the range of parameters leading to the formation of slugs (see discussion further), the error can not be higher than 40%. Finally, note that different ways to take into account and even estimate the viscosity value could be imagined such as the study of the relation between slug mass and flow rate. This is however outside the scope of the present paper.

4.2. Range of applicability of the slugs test

The first obvious limitation of the use of slugs test is that it requires the occurrence of a so-called slug-by-slug flow at the nozzle level. We call here a slug-by-slug flow, an unstable flow regime that leads to the formation of successive slugs. For a given material, the theoretical relations presented in the present paper do suggest that two main parameters can affect the typology of flow and the slugs formation: the extrusion speed and the nozzle diameter.

We study here the conditions required to form slugs at the nozzle level. Depending on the rheological properties of the printable mortar and the flow parameters, different flow typologies, represented in figure 8, can occur. The transition between these different typologies can be described more precisely by introducing two characteristic times t_n and t_c, respectively the necking time and the undeformed extrusion time. The necking phenomenon is the striction, which predates the separation of a slug. It is named after the well-known phenomenon, which occurs in the traditional direct tensile testings on steel specimens for instance. The necking time is defined as the time between the onset of the necking and the time of separation of the slug. It thus depends on both yield stress and viscosity of the extruded material. The undeformed extrusion time is the time required to extrude the amount of material needed to initiate the necking phenomenon. It depends on both yield stress and extrusion speed. The

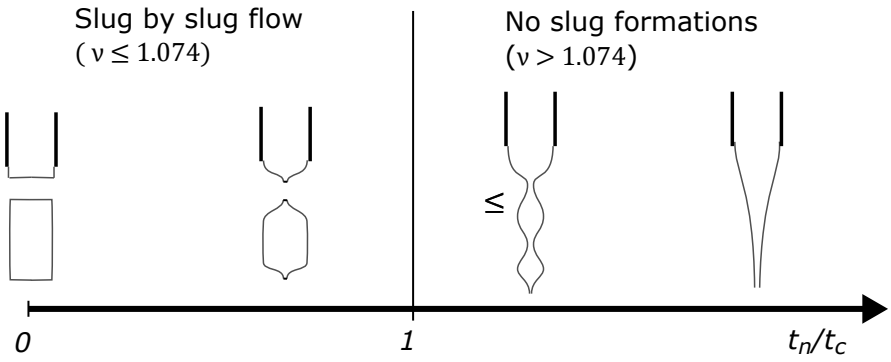

Figure 8: Different types of flow at nozzle exit. From left to right: the brittle discontinuity, the slug-by-slug flow, the multi-necking flow, the common viscous extensional flow.

flow typology goes from a pure viscous extensional flow characterized by $t_c = 0$, to a brittle fracture where no necking is observed, i.e. $t_n = 0$. Note that the presence of flow instabilities is not always sufficient to produce a proper slug-by-slug flow. It also requires that the slugs detaches, which happens only when the necking time is smaller than the underformed extrusion time $t_n < t_c$.

Using the theoretical analysis provided in [11], both undeformed extrusion time and necking time can be computed from the diameter evolution of the necking region in the Bingham fluid case. Details of the calculations are provided in appendix A. From this analysis, the domain of the slug-by-slug flow can be plotted as a function of the rheological parameters τ_c and μ_p and the extrusion velocity V. The non dimensional limits of slug-by-slug flow is plotted in blue line in figure 9.

Note that the brittle discontinuity relates to a fracture-type phenomenon and is therefore very different from necking. It can be expected to occur for large yield stress values and for mortar displaying a granular-type behavior. As such, it is strongly related to the presence of defects in the micro-structure. Only the necking phenomenon, as shown in figure 2-b,c,d. is related to flow onset and directly relates to yield stress. Consequently, in case of a brittle discontinuity, the computed yield stress would be expected to provide qualitative

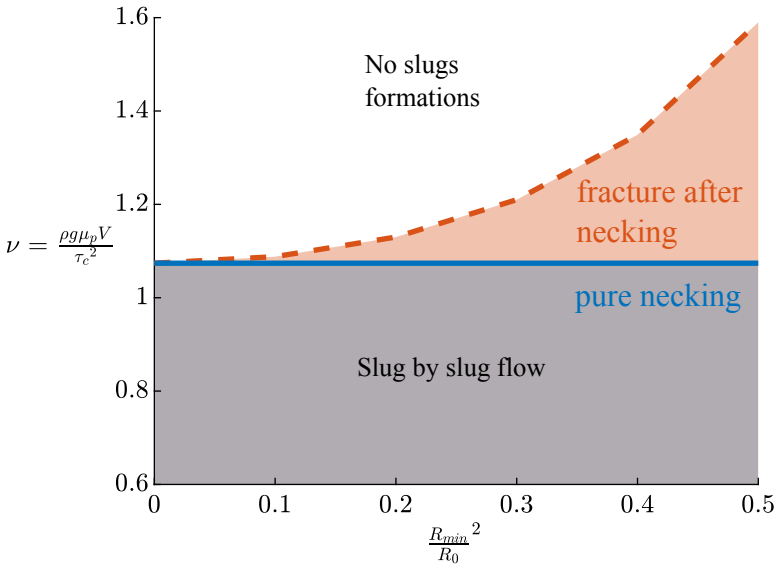

Figure 9: Domain of existence of slug formation

and potentially comparative information, but no quantitative assessment of the yield stress value (at least from a von Mises plasticity criterion point of view). Consequently, the transition between brittle discontinuity and necking is another limitation to the use of slugs-test for yield stress assessment.

Moreover, this brittle to ductile transition is somehow related to the limit of validity of the von Mises criterion to describe the end of the elastic domain of the printed mortar. Although this criterion, which implies a symmetrical behaviour between pure compression and pure traction, is widely accepted at fresh state, it is well-known that it is not adapted to the hardened state, where concrete shows significantly lower tensile strength in comparison with compressive strength. Printable materials being transition or structurating materials located between non-Newtonian pastes and quasi-solids, the slugs-test analysis could reach a limit for stiff materials. Furthermore, first experimental observations of a lower value of tensile strength compared to compressive strength on firm printable mortar at fresh state were recently reported suggesting a brittle failure in tension

[15].

Another interesting observation made during our experiments is the fact that smaller nozzle diameters seem to enhance the domain of existence of the slug-by-slug flow (see figure 9). To explain this phenomenon, we propose here an explanation of this feature based on the occurrence of a brittle fracture interrupting the pure visco-plastic necking and allowing for the detachment of the slug. Within this frame, we first assume that fracture initiation is independent from the bulk rheological behaviour and the nozzle size R_0, but finds its origin into the presence of some internal defects of a characteristic size noted R_{min}. The fracture, corresponding to the slug detachment, would then happen sooner after the initiation of the necking when the size of the defects R_{min} are getting closer to the size of nozzle R_0. Consequently, smaller nozzle diameter would therefore lead to larger domain of existence for the slug-by-slug flow. This explanation is computed mathematically in the appendix. The actual extension of the slug-by-slug domain is shown by the orange dotted line in figure 9.

4.3. Toward an homogeneity assessment for multi-component 3D printing process through the use of slugs test

We discuss here the ability of the automated slugs-test to assess the homogeneity of the tested material from the dispersion of the slugs' masses. The experimental results in table 1 show that the coefficient of variation (the ratio between standard variation and mean value) is higher when PAM is continuously added and dispersed in the printed mortar just before the nozzle exit (mix number 6 and 7). We suggest that this higher coefficient of variation finds its origin in the difficulties met when dispersing such a high molecular mass molecule in the printable mortar. As an illustration, the distributions of the mix 4 and 6, which have roughly the same yield stress are plotted in figure 10 as well as the fitted Gaussian distribution. This feature suggests that the measured coefficient of variation of the slugs mass distribution may give further information on the homogeneity of the material at the nozzle exit. The slugs test would be, in this case, an extremely useful tool to control and tune the dispersion into the initial

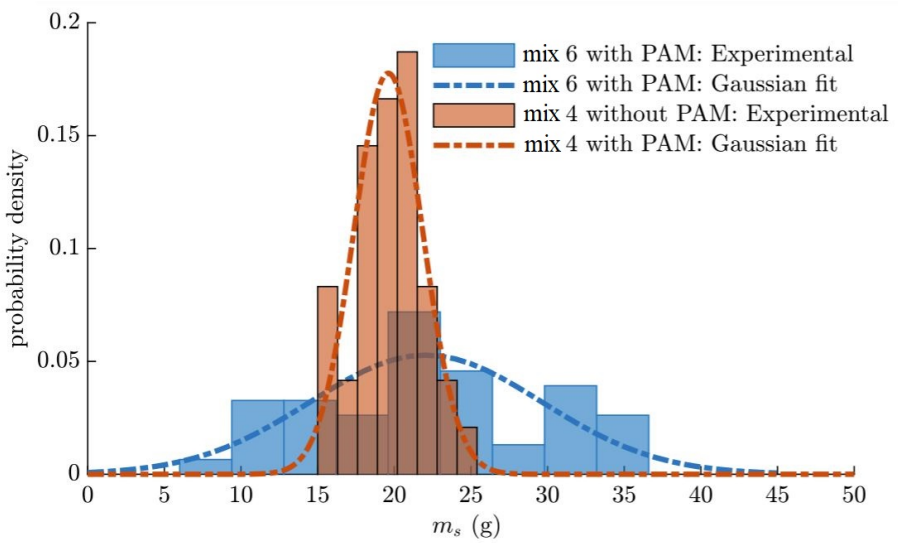

Figure 10: Slug mass distributions obtained from the automated slugs test with continuous dispersion of PAM (Polyacrylamide) in the printing head (exp 6) or without (exp 4)

mortar of a secondary material such as additives, solid particles or even short fibers, in a multi-component 3D printing process context.

4.4. Proposed protocol of the slugs test

One of the originality of the slugs-test compared to other rheological measurement methods is the considerable number of measurements done over a short period of time. With the set-up used for our experiments, which is close to industrial facilities, the period between two slugs is roughly one second. It is therefore possible to collect a large sample (30-100) of *slugs* in a short time span.

The measurement of slugs masses can therefore be considered as the sampling of a random variable. In the following, we assume a normal distribution for the slug masses. Since yield stress and slug mass are related by a linear relation, this means that the estimation of yield stress also follows a normal distribution. Depending on the context, in which the test is used, different statistical tools can be applied. In a scientific context, the construction of a confidence interval for

the yield stress assessment seems to be the most useful application. In industry, hypothesis tests may be more adequate and useful on daily practice basis.

4.5. Proposed protocol for homogeneity/uniformity assessment

In research, the aim of the test presented in this article is expected to be, first and foremost, to measure a yield stress and estimate a confidence interval for such a measurement although the variance (i.e. the material heterogeneity) is unknown. For that reason, we suggest here to assess the confidence interval from Student's law of degree $(n-1)$, where n is the number of slugs. We write $\overline{\tau} = \frac{1}{n}\sum_{i=1}^{n}\tau_i$ the empirical mean value and $s^* = \sqrt{\frac{1}{n-1}\sum_{i=1}^{n}(\tau_i - \overline{\tau})}$, the empirical standard deviation, and $t^* = t_\alpha(k)$ Student's t distribution. The confidence interval I_α is then defined as follows:

$$I_\alpha = \left[\overline{\tau} - t_\alpha(n-1)\cdot\frac{s^*}{\sqrt{n}}; \overline{\tau} + t_\alpha(n-1)\cdot\frac{s^*}{\sqrt{n}}\right] \tag{5}$$

The estimation of the mean slugs mass under the assumption of a normal distribution of slugs mass rapidly converges. The results of the automated slug tests are shown in Figure 11.

Figure 12 displays the size of the 95% confidence interval for the mean estimator normalized with the empirical mean. It clearly shows an asymptotic convergence to zero of all the intervals in our experiments. It should also be noticed that, with 30 slug measurements, the normalized size of the 95% is less than 5%, a satisfying accuracy in practice. This suggests that a few tens of slugs may be sufficient in most cases.

This estimator is built under the assumption that all mass measurements are independent. Off course, some noise could come from the balance, but also from other factors, more relevant to the end-user, like potential periodic variations in flow rate, due to feedback loop on pumps in the printing head. In that case, the estimators for variance should be changed. Potential for improvement include signal auto-correlations, which could help to identify possible changes in the extrusion flow during the test.

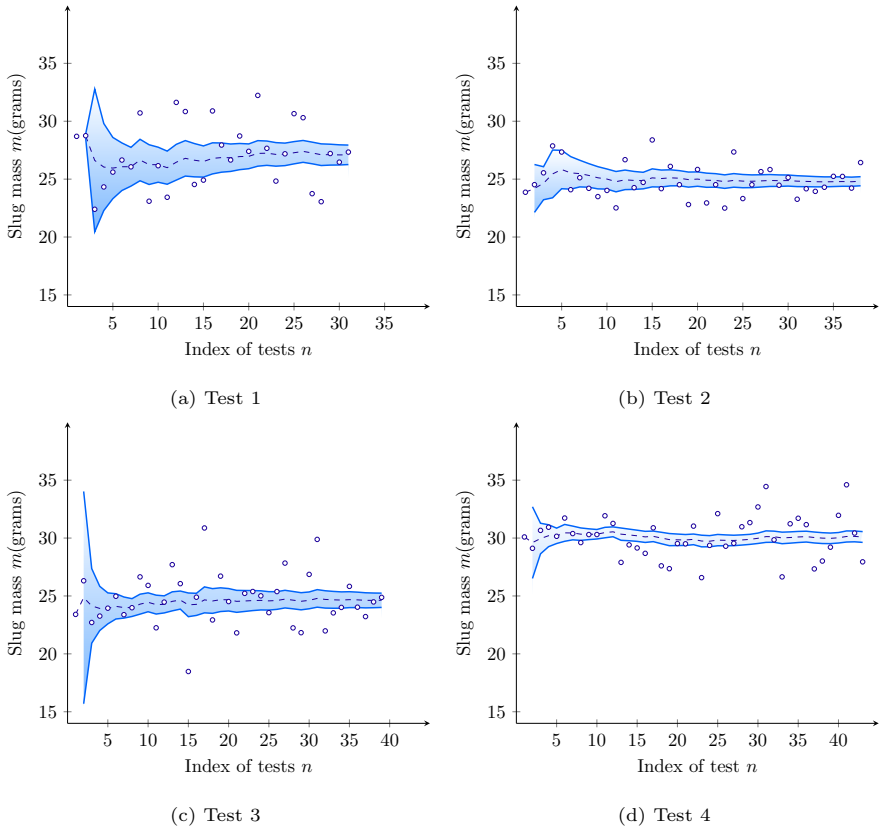

(a) Test 1

(b) Test 2

(c) Test 3

(d) Test 4

Figure 11: Iterative construction of the confidence interval for the slug mass m with respect to the number of samples n. The empirical mean of the slugs mass is represented by a dashed dark line, the confidence interval at 95% is shown as a shaded region. Individual measurements of the mass are shown as blue circles.

4.6. Proposed protocol to comply with the constraints of the manufacturing process

In practice, from a quality control point of view, industry is more likely to be interested into defining a range of admissible yield stress for a given printing process. The lower bound for yield stress τ_{min} would then come from buildability requirements (the ability of a layer to support its own weight and the weight of the others), while higher bound τ_{max} might come from pumpability requirements [3], from shaping requirements in the case of curved filaments with variable

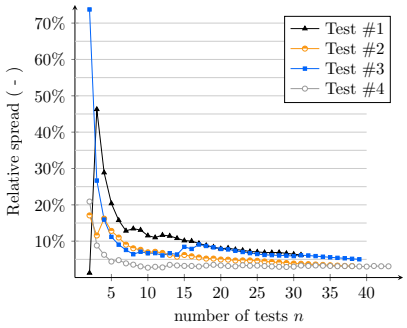

Figure 12: Size of the 95% confidence interval normalized with the empirical mean.

thickness [6], or from strength requirements of the layers underneath in case of layer squeezing [5]. Therefore, an industry engineer is more likely to test two hypotheses, written H_0 and H_1 in equation (6).

$$\begin{aligned} \mathrm{H}_0 &: \tau > \tau_{min} \\ \mathrm{H}_1 &: \tau < \tau_{max} \end{aligned} \tag{6}$$

Such hypotheses can then be tested with Student's $t-$test. The random variable of the t-test reads:

$$z = \begin{cases} \sqrt{n}\dfrac{\overline{\tau}_n - \tau_{min}}{s_n^*} & \text{for } \mathrm{H}_0 \\ \sqrt{n}\dfrac{\overline{\tau}_n - \tau_{max}}{s_n^*} & \text{for } \mathrm{H}_1 \end{cases} \tag{7}$$

$$\text{where: } s_n^* = \sqrt{\frac{1}{n-1}\sum_{i=1}^{n}(\tau_i - \overline{\tau}_n)^2}$$

On one hand, the hypothesis H_0 is rejected when z is less than the α order quantile of Student's Law at $n-1$ degrees of freedom. On the other hand, the hypothesis H_1 is rejected when z is greater than the quantile of order $1-\alpha$ of Student's Law at $n-1$ degrees of freedom. Naturally, the value of α needs to be adapted to a defined risk of failure during the production.

5. Conclusions and perspectives

To conclude, we introduced in this paper a simple test for direct inline assessment of yield stress of printable mortar at the nozzle exit. Two experimental

validations were proposed. The first one was done manually using a simple lab extruder. The second one was carried using an automatized device integrated in a large scale 3D-printing facilities of the École des Ponts ParisTech. The latter allows for an automatic assessment of yield stress and the associated confidence interval. In both cases, a good correlation between measurements done by the slugs-test and those made by traditional slump test was obtained. The limits of applicability of the test has been thoroughly studied as well as the estimation of the error made when neglecting viscosity effects. This study showed that the overestimation of the yield stress value would be always inferior to 40% and often around 10% for usual printing systems. We also highlighted the presence of a regime of brittle fracture for very stiff materials. Finally, we suggested that the slugs-test is also potentially able to provide information of the printable material homogeneity. That would be particularly interesting when additives, such as accelerators or fibers are continuously added and dispersed into the material at the level of the print head.

Appendix A. Domain of existence of discontinuous flow

The theoretical work of [11] provides the differential equation modelling the radius evolution for a Herschel-Bulkley fluid. For simplicity reason, only the Bingham fluid case, i.e. $n = 1$ and $K = \mu_p$, is studied here. In the international system of units, the differential equation reduces to:

$$\dot{R} = -\frac{R}{2\sqrt{3}} \left(\frac{\rho g L R_0^2}{\sqrt{3}\mu_p R^2} - \frac{\tau_c}{\mu_p} \right) \tag{A.1}$$

where L is the length of the material under the necking section. Studying the case where it is taken equal to the actual length of the final slug given by equation (3), i.e. $L = L_s$, it admits a analytical solution noted :

$$R(t) = \sqrt{A e^{\frac{\tau_c}{\sqrt{3}\mu_p} t} + \frac{\rho g {R_0}^2}{\sqrt{3}\tau_c} L_s} \tag{A.2}$$

where A is a constant which can be evaluated using the fact that the initial radius is equal to the nozzle one :

$$\begin{aligned} R(0) &= \sqrt{A + \frac{\rho g {R_0}^2}{\sqrt{3}\tau_c} L_s} = R_0 \\ \implies A &= {R_0}^2 - \frac{\rho g {R_0}^2}{\sqrt{3}\tau_c} L_s \end{aligned} \tag{A.3}$$

The final expression of the radius is the necking zone is given by :

$$R(t) = R_0 \sqrt{\left(1 - \frac{L_s}{L_c}\right) e^{\frac{\tau_c}{\sqrt{3}\mu_p} t} + \frac{L_s}{L_c}} = \sqrt{(1 - \lambda_b)\, e^{\frac{\tau_c}{\sqrt{3}\mu_p} t} + \lambda_b} \tag{A.4}$$

Supposing that the actual separation due to fracture occurs when $R = R_{min}$, the necking time t_n can be computed resolving $R(t) = R_{min}$, it yields:

$$t_n = \frac{\sqrt{3}\mu_p}{\tau_c} \ln \left(\frac{\lambda_b - \left(\frac{R_{min}}{R_0}\right)^2}{\lambda_b - 1} \right) \tag{A.5}$$

Consequently, in the Bingham case, the borderline between the slug-by-slug flow and the absence of slugs is given by :

$$t_n = t_c \tag{A.6}$$

$$\implies \frac{\sqrt{3}\mu_p}{\tau_c} \ln \left(\frac{\lambda_b - \left(\frac{R_{min}}{R_0}\right)^2}{\lambda_b - 1} \right) = L_c/V = \frac{\sqrt{3}\tau_c}{\rho g V} \tag{A.7}$$

$$\implies \nu \ln \left(\frac{\frac{1+\sqrt{1+4\nu}}{2} - \left(\frac{R_{min}}{R_0}\right)^2}{\frac{\sqrt{1+4\nu}-1}{2}} \right) = 1 \tag{A.8}$$

Equation (A.8) provides the maximal values of ν to obatin the slug-by-slug flow, depending on the fracture radius-to-nozzle radius ratio. If no fracture occurs during necking, $\frac{R_{min}}{R_0} = 0$ and ν reduces to 1.074.

References

[1] V. Mechtcherine, F. Bos, A. Perrot, W. L. da Silva, V. Nerella, S. Fataei, R. Wolfs, M. Sonebi, N. Roussel, Extrusion-based additive manufacturing

with cement-based materials – Production steps, processes, and their underlying physics: A review, Cement and Concrete Research 132 (2020) 106037. doi:10.1016/j.cemconres.2020.106037.
URL https://linkinghub.elsevier.com/retrieve/pii/S0008884619317132

[2] R. Duballet, Building systems in robotic extrusion of cementitious materials, Ph.D. thesis, Université Paris-est (Dec. 2018).

[3] N. Roussel, Rheological requirements for printable concretes, Cement and Concrete Research 112 (2018) 76–85. doi:10.1016/j.cemconres.2018.04.005.
URL http://linkinghub.elsevier.com/retrieve/pii/S000888461830070X

[4] B. F. S. H. L. D. H. N. K. H. M. V. W. T. R. N. Buswell R.A., Leal da Silva W.R., A process classification framework for defining and describing digital fabrication with concrete, Cement and Concrete Research 134 (2020) 106068. doi:10.1016/j.cemconres.2020.106068.
URL https://www.sciencedirect.com/science/article/pii/S0008884619316709?via%3Dihub

[5] P. Carneau, R. Mesnil, N. Ducoulombier, O. Baverel, N. Roussel, Geometrical and mechanical characterisation of the Oriented Lace Pressing Strategy for 3d printing, in: DC 2020, RILEM Bookseries 28, Vol. (under review), F. P. Bos et al. (Eds.), Eindhoven University of Technology, 2020.

[6] P. Carneau, R. Mesnil, N. Roussel, O. Baverel, Additive manufacturing of cantilever - From masonry to concrete 3D printing, Automation in Construction 116 (2020) 103184. doi:10.1016/j.autcon.2020.103184.
URL https://linkinghub.elsevier.com/retrieve/pii/S0926580519308568

[7] M. R. C. J.-F. Demont L., Ducoulombier N., Flow-based pultrusion of continuous fibers for cement-based composite material and additive

manufacturing: rheological and technological requirements, Composite Structures 262 (2021) 113564. doi:10.1016/j.compstruct.2021.113564.
URL https://www.sciencedirect.com/science/article/abs/pii/S0263822321000258

[8] N. Ducoulombier, P. Carneau, R. Mesnil, L. Demont, J.-F. Caron, N. Roussel, "The Slug Test": Inline Assessment of Yield Stress for Extrusion-Based Additive Manufacturing, in: F. P. Bos, S. S. Lucas, R. J. Wolfs, T. A. Salet (Eds.), Second RILEM International Conference on Concrete and Digital Fabrication, Vol. 28, Springer International Publishing, Cham, 2020, pp. 216–224, series Title: RILEM Bookseries. doi:10.1007/978-3-030-49916-7_22.
URL http://link.springer.com/10.1007/978-3-030-49916-7_22

[9] C. Gosselin, R. Duballet, P. Roux, N. Gaudillière, J. Dirrenberger, P. Morel, Large-scale 3D printing of ultra-high performance concrete – a new processing route for architects and builders, Materials & Design 100 (2016) 102–109. doi:10.1016/j.matdes.2016.03.097.
URL https://linkinghub.elsevier.com/retrieve/pii/S0264127516303811

[10] R. Wolfs, F. Bos, T. Salet, Correlation between destructive compression tests and non-destructive ultrasonic measurements on early age 3D printed concrete, Construction and Building Materials 181 (2018) 447–454. doi:10.1016/j.conbuildmat.2018.06.060.
URL https://linkinghub.elsevier.com/retrieve/pii/S0950061818314508

[11] P. Coussot, F. Gaulard, Gravity flow instability of viscoplastic materials: The ketchup drip, Physical Review E 72 (3) (Sep. 2005). doi:10.1103/PhysRevE.72.031409.
URL https://link.aps.org/doi/10.1103/PhysRevE.72.031409

[12] R. Wolfs, F. Bos, T. Salet, Early age mechanical behaviour

of 3D printed concrete: Numerical modelling and experimental testing, Cement and Concrete Research 106 (2018) 103–116. doi:10.1016/j.cemconres.2018.02.001.
URL http://linkinghub.elsevier.com/retrieve/pii/S000888461730532X

[13] H. Bessaies-Bey, R. Baumann, M. Schmitz, M. Radler, N. Roussel, Effect of polyacrylamide on rheology of fresh cement pastes, Cement and Concrete Research 76 (2015) 98–106. doi:10.1016/j.cemconres.2015.05.012.
URL https://linkinghub.elsevier.com/retrieve/pii/S000888461500143X

[14] N. Roussel, P. Coussot, "Fifty-cent rheometer" for yield stress measurements: From slump to spreading flow, Journal of Rheology 49 (3) (2005) 705–718. doi:10.1122/1.1879041.
URL http://sor.scitation.org/doi/10.1122/1.1879041

[15] Y. Jacquet, V. Picandet, D. Rangeard, A. Perrot, Gravity Driven Tests to Assess Mechanical Properties of Printable Cement-Based Materials at Fresh State, in: F. P. Bos, S. S. Lucas, R. J. Wolfs, T. A. Salet (Eds.), Second RILEM International Conference on Concrete and Digital Fabrication, Vol. 28, Springer International Publishing, Cham, 2020, pp. 280–289, series Title: RILEM Bookseries. doi:10.1007/978-3-030-49916-7_29.
URL http://link.springer.com/10.1007/978-3-030-49916-7_29